Electronic Supplementary Material (ESI) for ChemComm.

Stability of Metal-Organic Frameworks under gamma irradiation

Christophe Volkringer[ab], Clément Falaise[a], Philippe Devaux[a], Raynald Giovine[a], Victoria Stevenson[a], Frédérique Pourpoint[a], Olivier Lafon[a], Mélanie Osmond[c], Caroline Jeanjacques[c], Benoit Marcillaud[c], Jean-Christophe Sabroux[c], Thierry Loiseau[a]

[a]Unité de Catalyse et Chimie du Solide (UCCS) – UMR CNRS 8181, Université de Lille, ENSCL, Bat C7, BP 90108, 59652 Villeneuve d'Ascq, France.

[b]Institut Universitaire de France, 1 rue Descartes, 75231 Paris Cedex 05.

[c]Institut de Radioprotection et de Sureté Nucléaire (IRSN), PSN-RES/SCA, Centre de Saclay, 91192 Gif sur Yvette, France.

Supporting information

Metal-Organic Framework

Synthesis

All the MOF synthesis was inspired from the literature and adapted to relative large scale production (0.5 to 4 gr of MOF per synthesis)

MOF acronym and anhydrous formula	Metal salt	ligand	solvent	heating process	activation	ref
MIL-53 Al(OH)bdc	$Al(NO_3)_3$, $9H_2O$ 3g	Terephthalic acid (H_2-bdc) 1.5g	H_2O (40ml)	210°C, 24h	DMF(40 ml),150°C (12h) and desolvation at 200°C (12h)	1
MIL-100 $Al_3O(OH)$ $(btc)_4$	$Al(NO_3)_3$, $9H_2O$ 7.48g	Trimesic acid (Me_3-btc) 3.39	H_2O (91 ml) + HNO_3 (1M, 25ml)	180°C, 3h	DMF (40ml), 150°C (5h) and desolvation at 300°C (5h)	2
MIL-120 $Al_4(OH)_8$(btec)	$Al(NO_3)_3$, $9H_2O$ 3.2g	Pyromellitic acid (H_4-btec) 0.5	H_2O (20ml) + NaOH (4M, 3.4ml)	210°C, 24h	H_2O (200ml), 100°C (5h) and desolvation at 150°C (12h)	3
HKUST-1 $Cu_3(btc)_2$	$Cu(NO_3)_2$, $3H_2O$ 3.5g	Trimesic acid (H_3-btc 2.1g	H_2O (36ml) + EtOH (36ml)	110°C, 12h	150°C, 16h	4
ZIF-8 $Zn(Im)_2$	$Zn(NO_3)_2$, 6H2O 0.6g	1-methylimidazole (H-Im) 0.32g	H_2O (3ml) + NH_4OH	RT, 10min	150°C, 16h	5
UiO-66 $Zr_6O_4(OH)_4(bdc)_6$	$ZrCl_4$ 1.1g	Terephthalic acid H_2-bdc 0.68g	DMF (60ml)	120°C, 24h	150°C, 16h	6

Structural characteristics and description

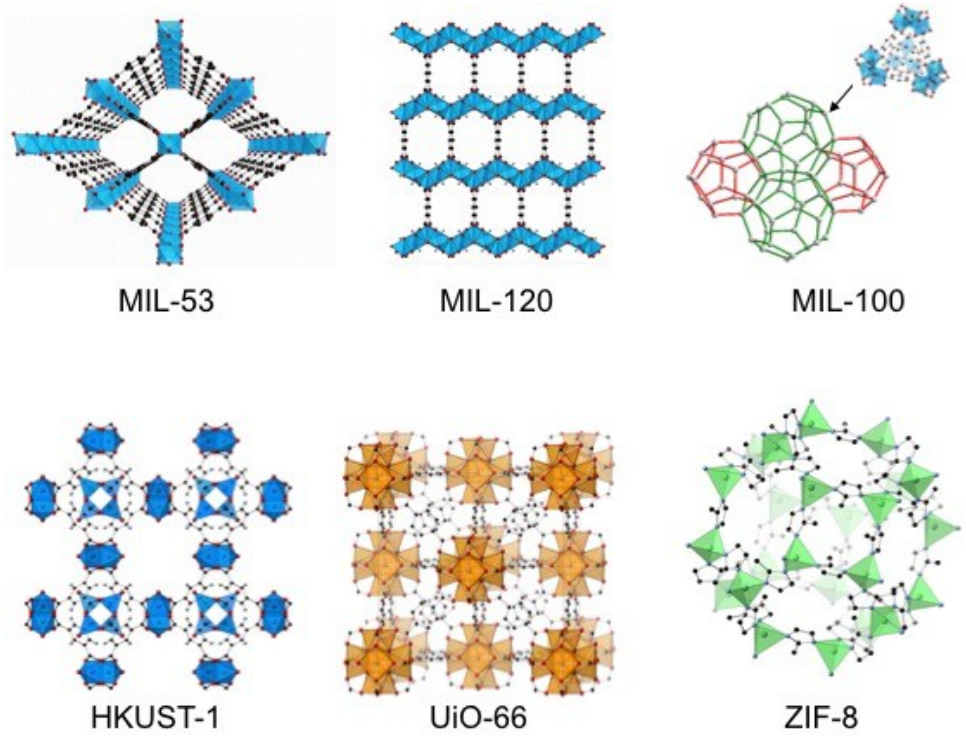

Figure S1: Illustration of the structures of the MOFs discussed in this work

MOF	Pore aperture(s) Å	cavity diameter(s) Å	Calculated density of the anhydrous solid (g/cm^3)
MIL-53	8	/	0.97
MIL-100	5.4 and 8.8	25 and 29	0.80
MIL-120	5.4 x 4.7	/	1.56
HKUST-1	/	5 and 13	1.08
ZIF-8	3.4	11.6	0.92
UiO-66	6	8 and 11	1.22

Table S1: Cross section calculation given in barns (b) per atom, where b = 10^{-24} cm^2

Metal	Energy (MeV)	Total attenuation (barns/atom)
Al	1.17	2.54
	1.33	2.38
Zr	1.17	7.98
	1.33	7.48
Cu	1.17	5.70
	1.33	5.35
Zn	1.17	5.90
	1.33	5.54
H	1.17	0.19
	1.33	0.18
C	1.17	1.17
	1.33	1.09
N	1.17	1.36
	1.33	1.28
O	1.17	1.56
	1.33	1.46

Picture

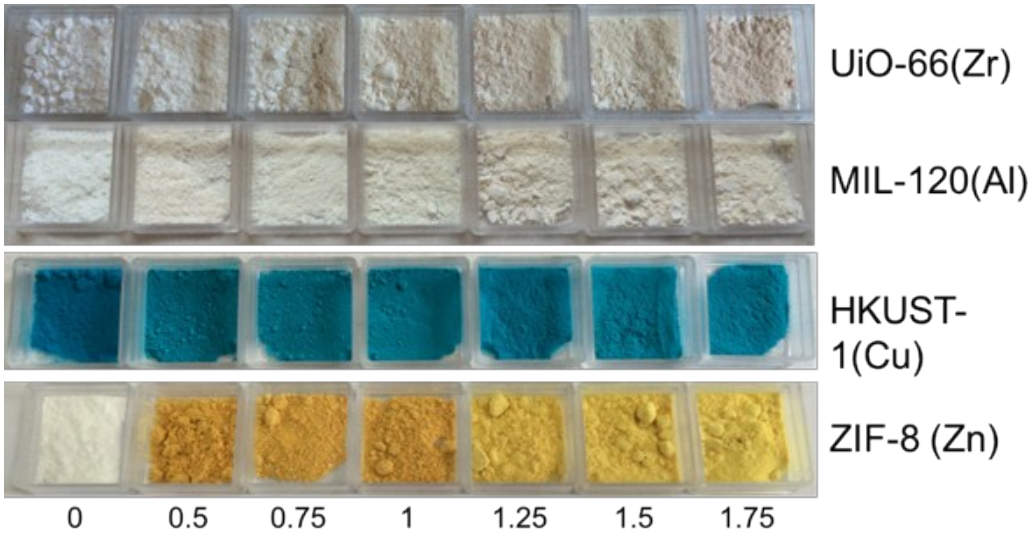

Figure S2a: Picture of MOF powders, illustrating the impact of irradiation MOF aspect

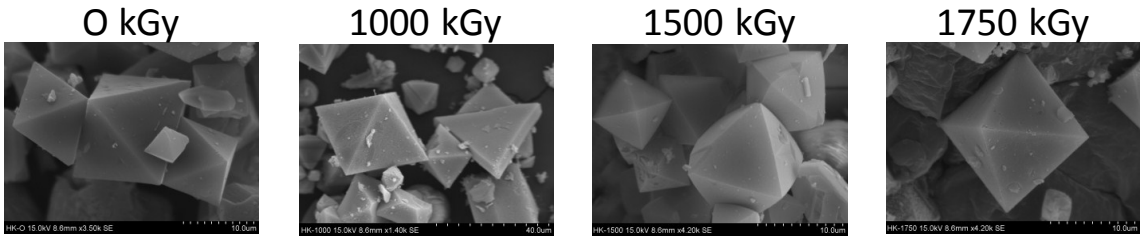

Figure S2b: SEM Picture of HKUST-1 MOF powders, for different doses of irradiation

IRMA facility

IRMA (Irradiation of MAterials) is a panoramic irradiation cell for studying how materials or equipment react to the effects of dose and dose rate due to exposure to gamma radiation.

The research facility hosts four cylindrical sealed sources of cobalt-60 (T½ = 5.27 years), totaling 1276 TBq as of January 2016. The dose rates at the test location can range from 5 µGy/h to 20 kGy/h. The radioactive sources are remotely handled after withdrawal from their safe repository (lead castle). The required number of ^{60}Co sources are then displayed in order to deliver the targeted dose rate to the items to be tested during a predetermined time (hence, the programed dose).

Figure S4a: the IRMA facility (Saclay Research Center)

Figure S4b: inside the irradiation cell (inner volume 24 m^3)

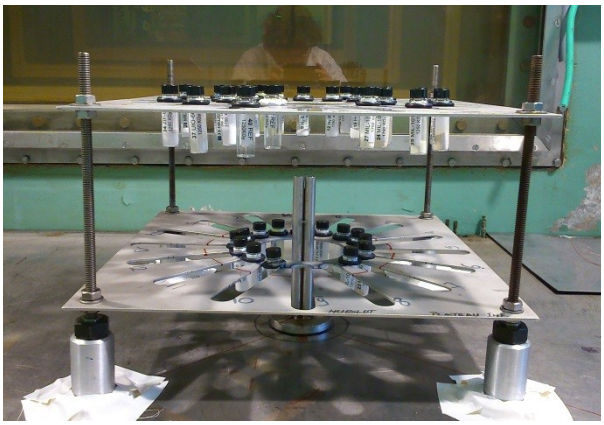

Figure S4c: MOF samples layout before irradiation

With the sources in the lead castle, the irradiation cell can be entered safely, thus offering a convenient roomy area for setting up the material samples or equipment (*e.g.*, printed circuit board) on the test bench. The test sequence for an irradiation experiment is as follows:

1- Selection of sources to be used, according to the targeted dose rate;
2- Calculation of the theoretical distances between the source(s) and the items under test using a dedicated software (Microshield®) to simulate the dose rate absorbed by air at the material samples or equipment locations;
3- Validation of the theoretical distances by measuring the dose rate (air equivalent) using calibrated ionization chambers (volume of chamber available ranging from 0,125 cm^3 to 3 L, in order to measure dose rates in the µGy/h to kGy/h ranges) at the location of the experimental mock-ups representative of the material under irradiation;
4- Installation in the irradiation cell of items to be tested at their test locations, as validated hereabove.
5- Placing of the source(s) on the test bench for the programed duration of irradiation.
6- Retrieval of the irradiated items after the test.

The irradiation cell is locked up during steps 3 and 5. Otherwise, the sources are safely stored in the lead castle. The cell is not contaminated: neither the cell nor the irradiated samples can be activated by the 1.332 MeV gamma emission of ^{60}Co.

Powder X-ray diffraction

The powder X-ray diffraction patterns were collected at room temperature with a D8 advance A25 Bruker apparatus with a Gragg-Brentano geometry. The D8 diffractometer is equipped with a LynxEye detector with $Cu_K\alpha_{1/}\alpha_2$ radiation. The 2θ range was 3-50° with a step of 0.02° and a counting time of 0.5 seconds per step.

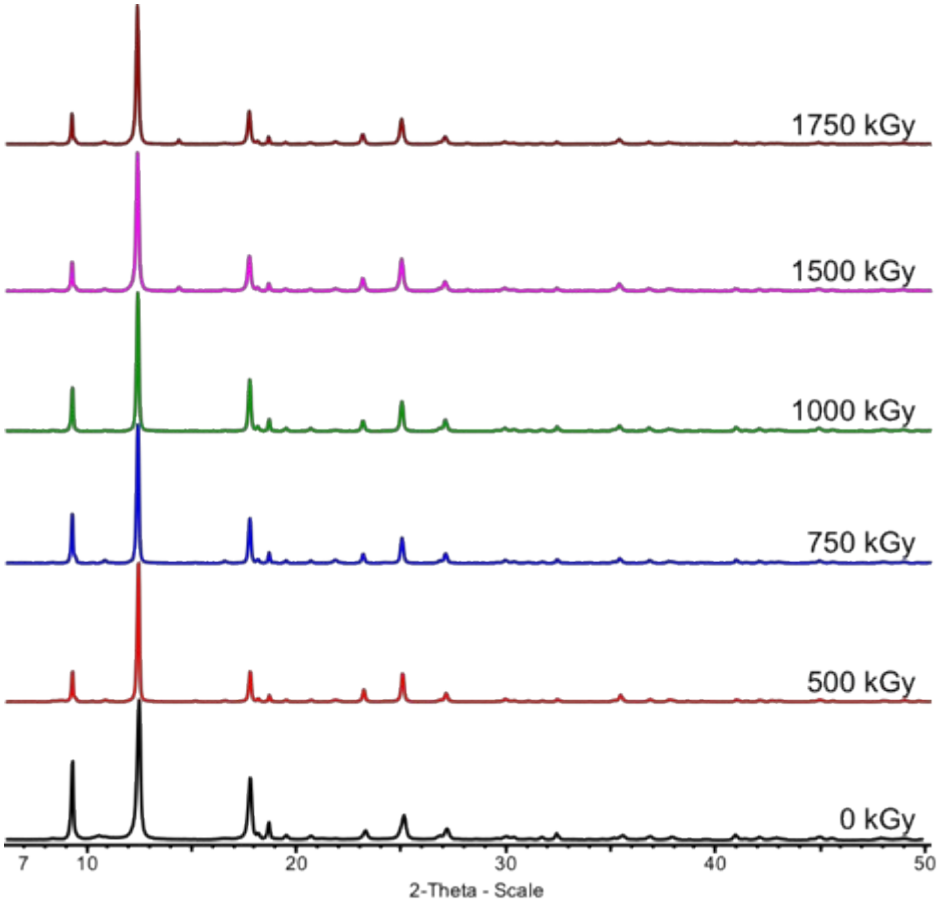

Figure S5a: Comparison of X-ray powder patterns of non-irradiated and irradiated MIL-53(Al)

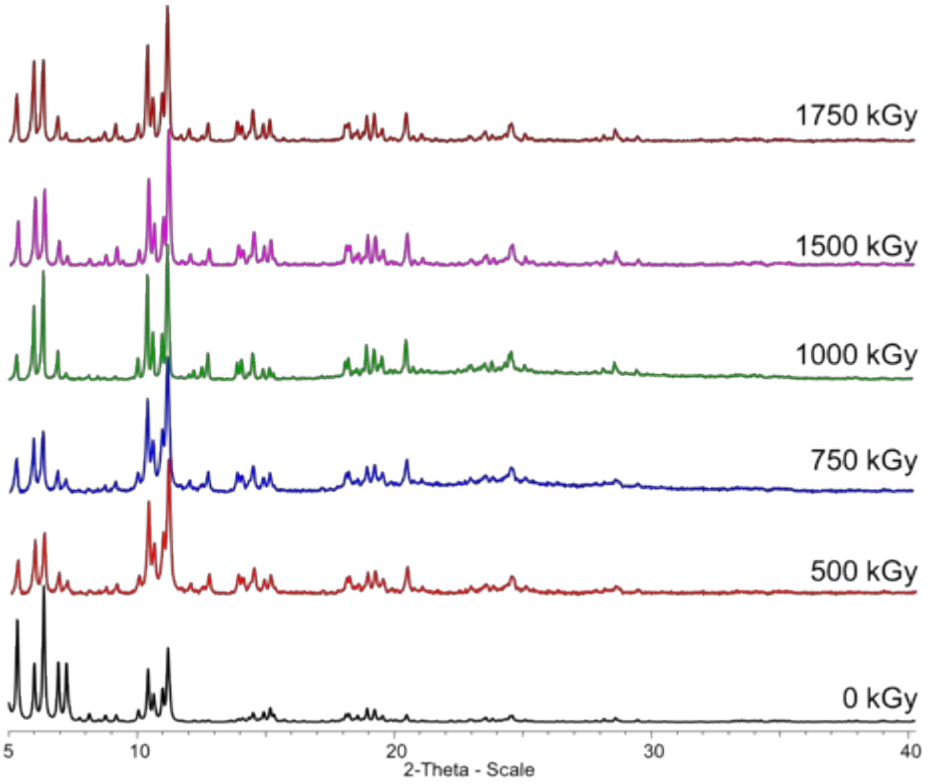

Figure S5b: Comparison of X-ray powder patterns of non-irradiated and irradiated MIL-100(Al)

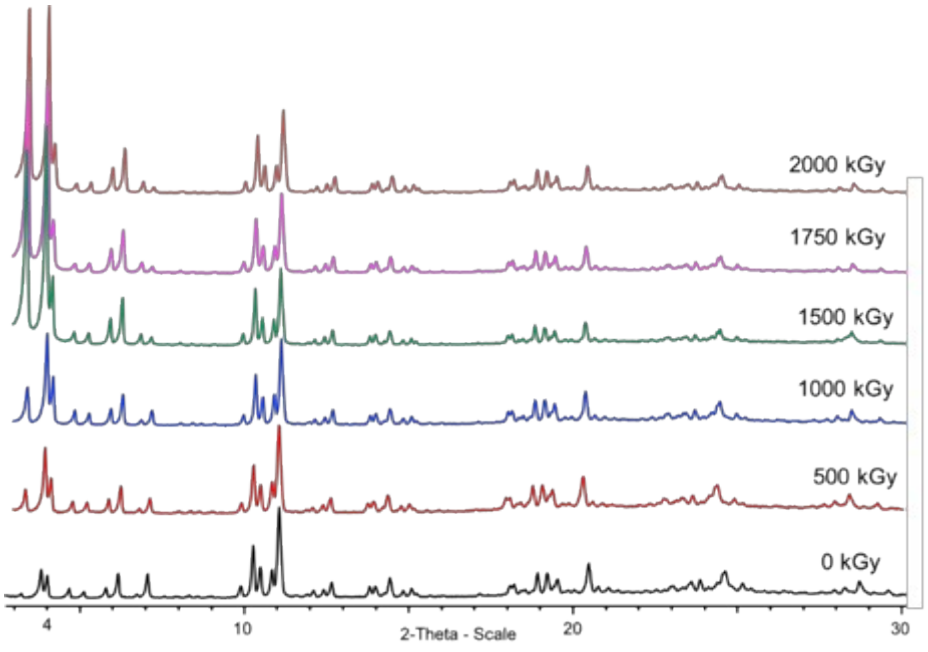

Figure S5c: Comparison of X-ray powder patterns of non-irradiated and irradiated MIL-100(Al)-as (as synthesized).

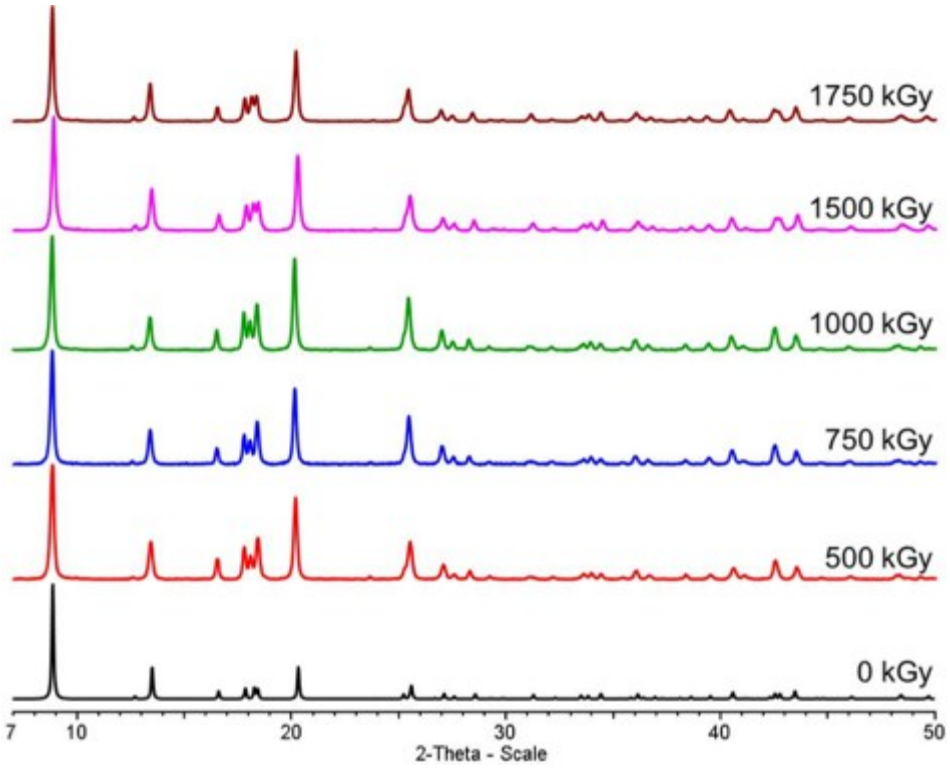

Figure S5d: Comparison of X-ray powder patterns of non-irradiated and irradiated MIL-120(Al)

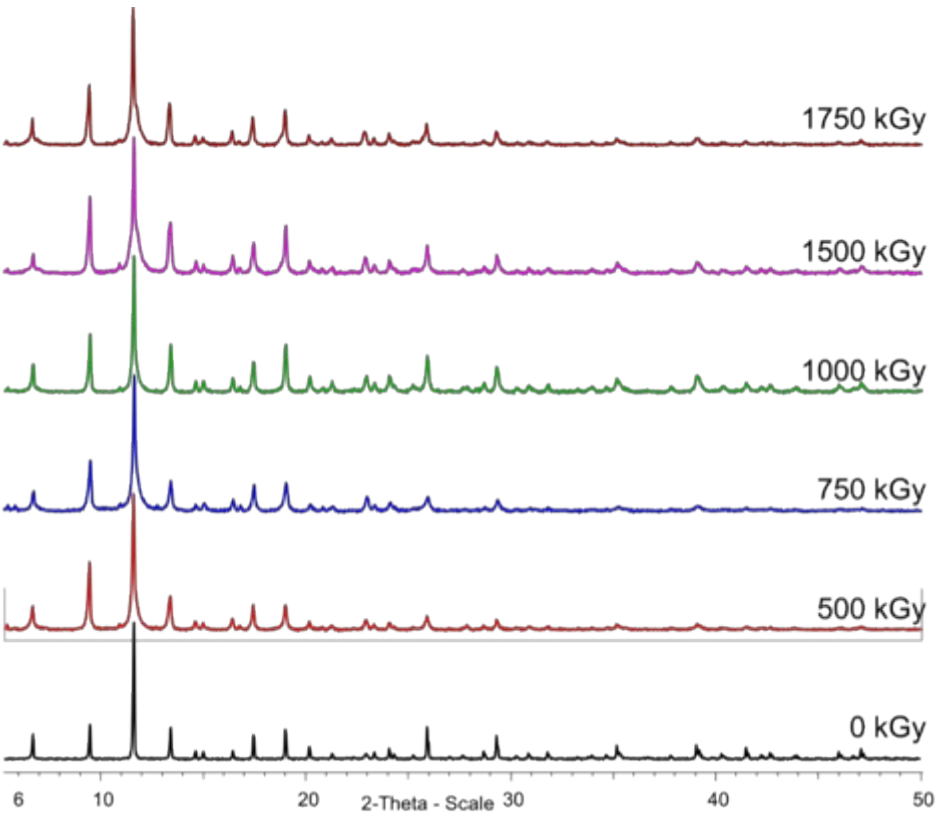

Figure S5e: Comparison of X-ray powder patterns of non-irradiated and irradiated HKUST-1

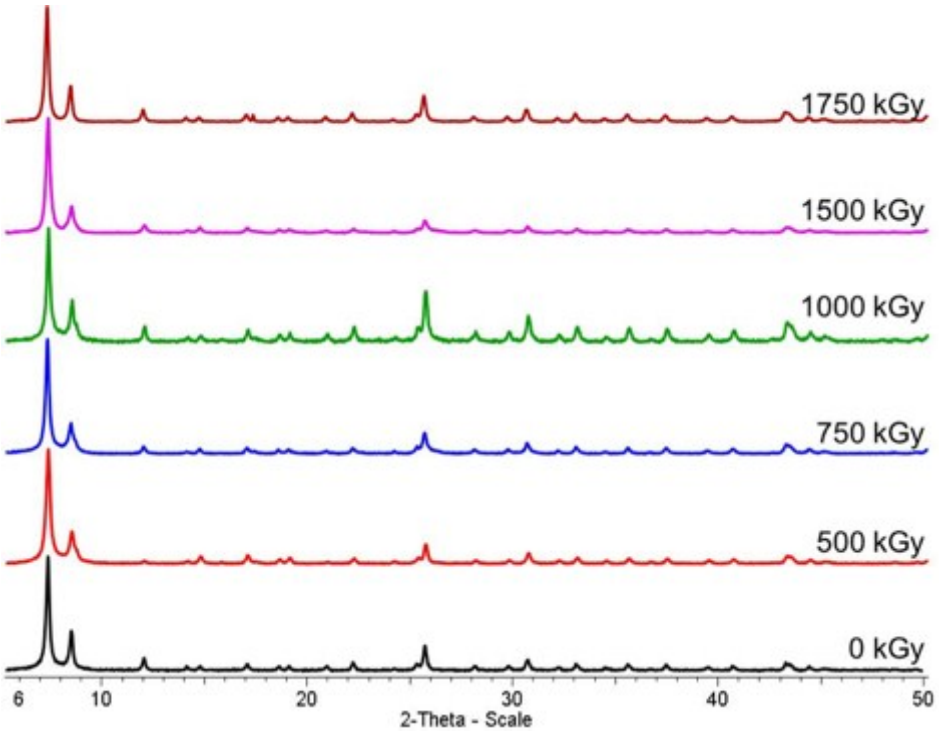

Figure S5f: Comparison of X-ray powder patterns of non-irradiated and irradiated UiO-66(Zr)

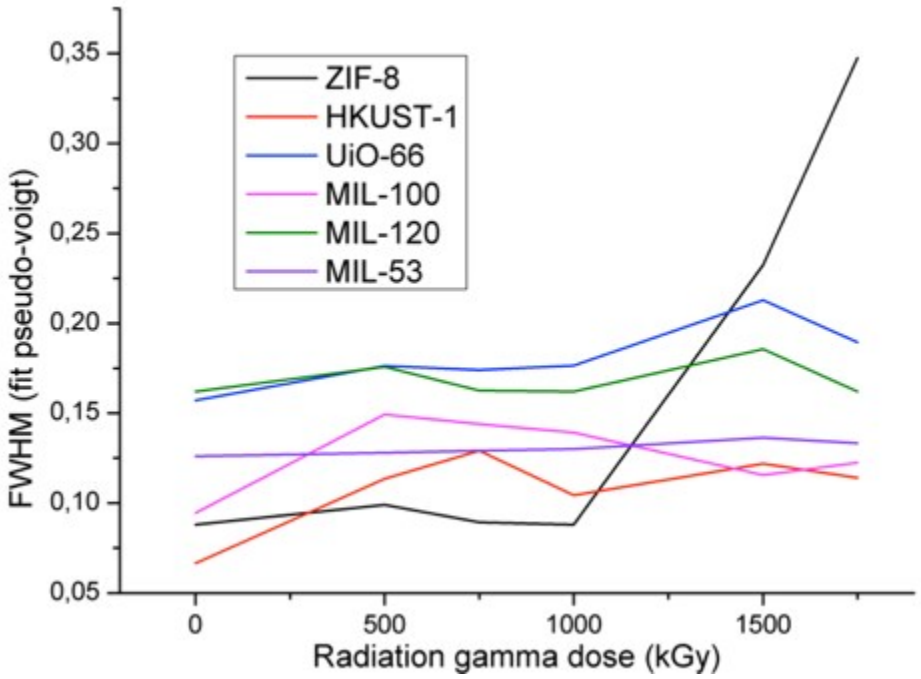

Figure S5g: evolution of the full width half maximum of powder X-ray diffraction peaks of the different MOFs as a function of irradiation dose

Gas sorption

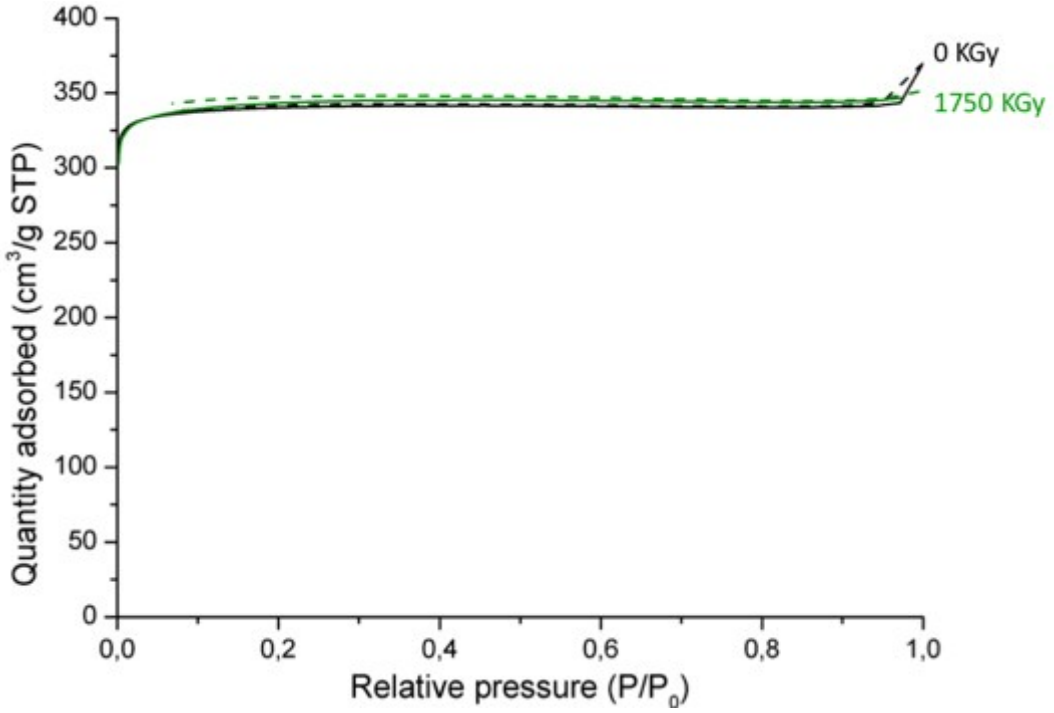

Figure S6a: Isotherm curves for the adsorption (solid) and desorption (dash) of nitrogen (77 K) in irradiated (1750 KGy) and non-irradiated MIL-53(Al)

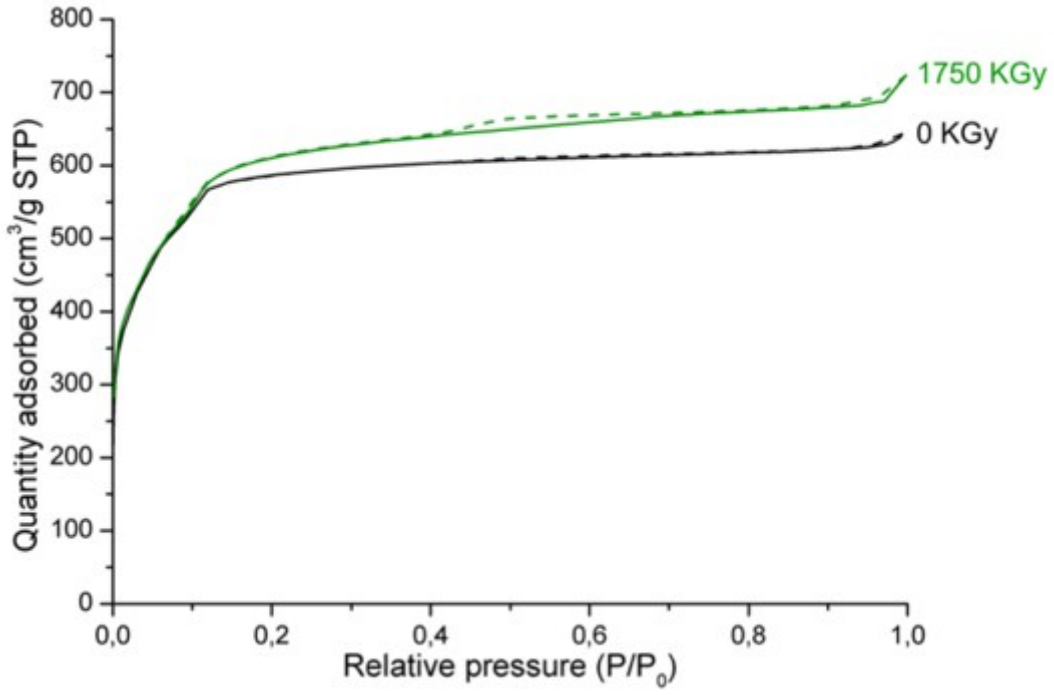

Figure S6b: Isotherm curves for the adsorption (solid) and desorption (dash) of nitrogen (77 K) in irradiated (1750 KGy) and non-irradiated MIL-100(Al)

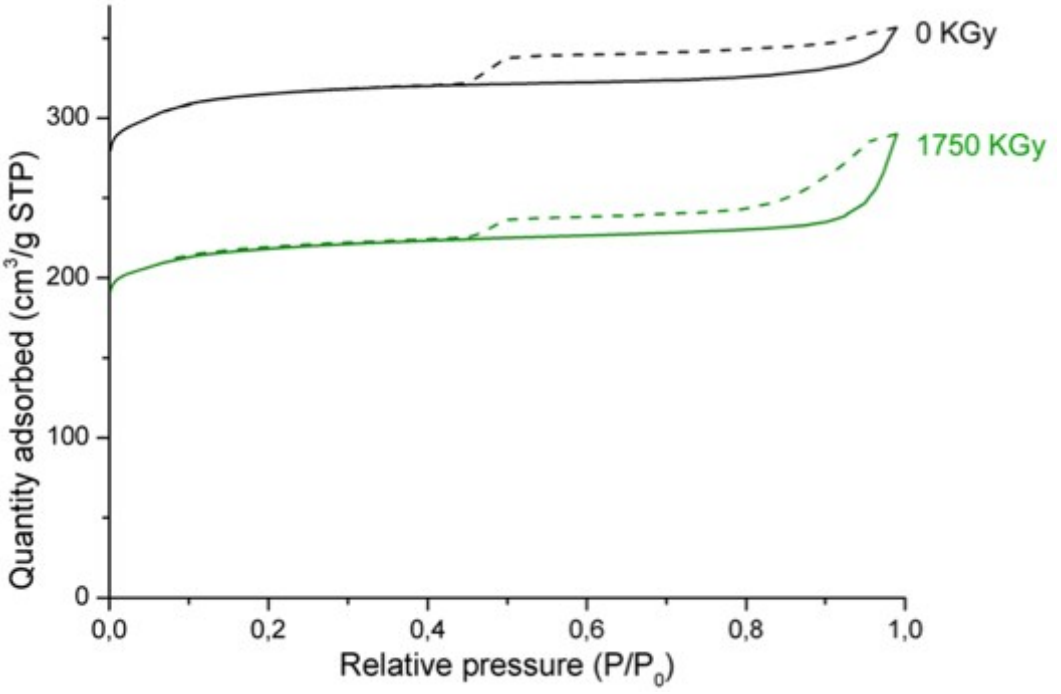

Figure S6c: Isotherm curves for the adsorption (solid) and desorption (dash) of nitrogen (77 K) in irradiated (1750 KGy) and non-irradiated HKUST-1(Cu)

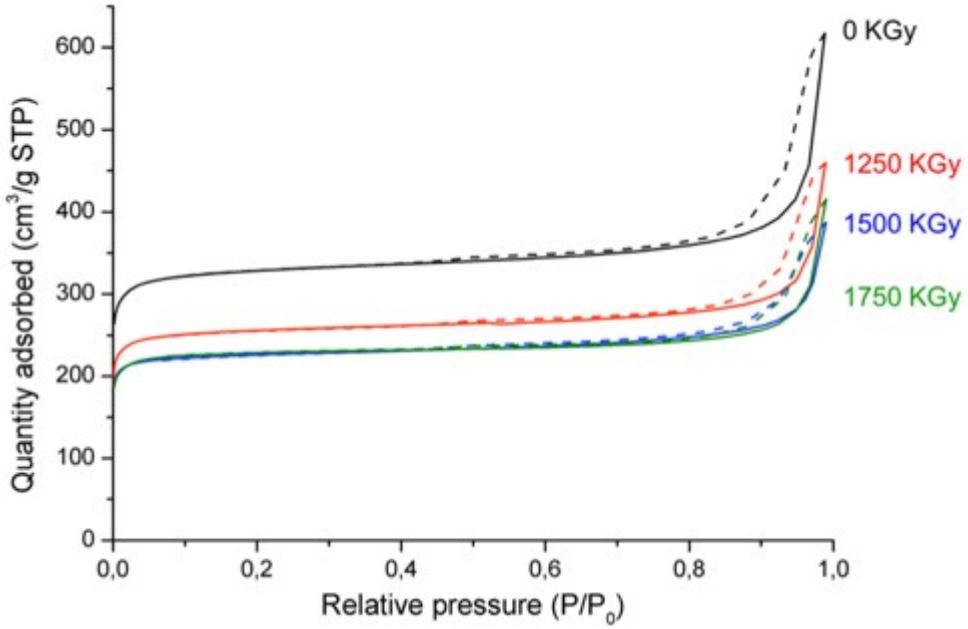

Figure S6d: Isotherm curves for the adsorption (solid) and desorption (dash) of nitrogen (77 K) in irradiated and non-irradiated UiO-66(Zr)

Table S2: Comparison between BET surface areas of irradiated (1750 kGy) and non-irradiated MOF

MOF	Irradiation dose (kGy)	BET surface (m^2/g)
MIL-53(Al)	0	1254
	1750	1264
MIL-100(Al)	0	2071
	1750	2286
MIL-120(Al)	0	145
	1750	417
HKUST-1(Cu)	0	1164
	1750	805
UiO-66(Zr)	0	1214
	1750	847
ZIF-8(Zn)	0	1326
	1750	598

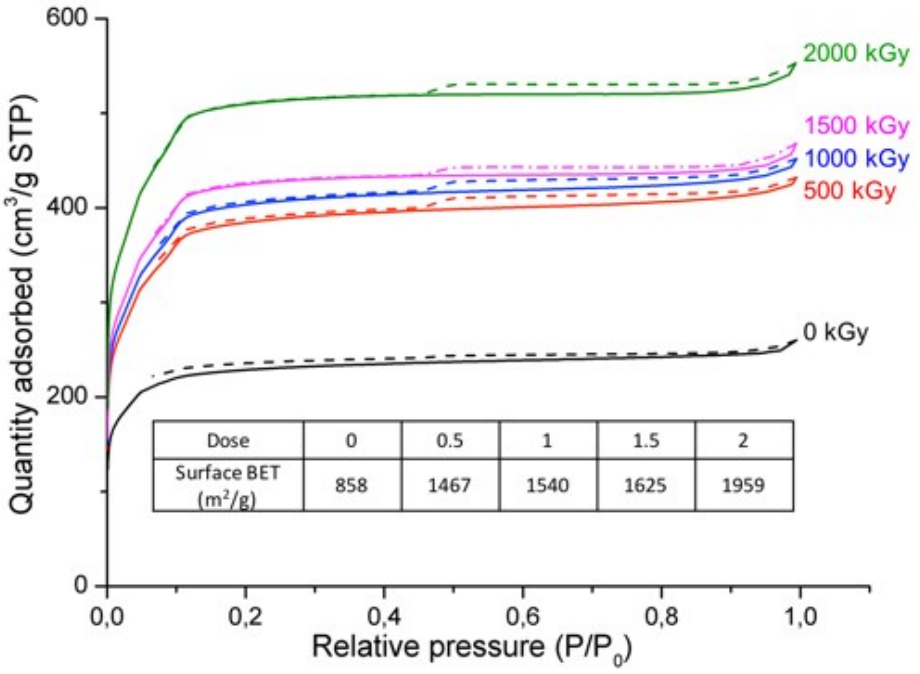

Figure S6e: Influence of gamma irradiation dose over as-synthesized MIL-100(Al) highlighted by Isotherm curves for the adsorption (solid) and desorption (dash) of nitrogen (77 K)

Infrared

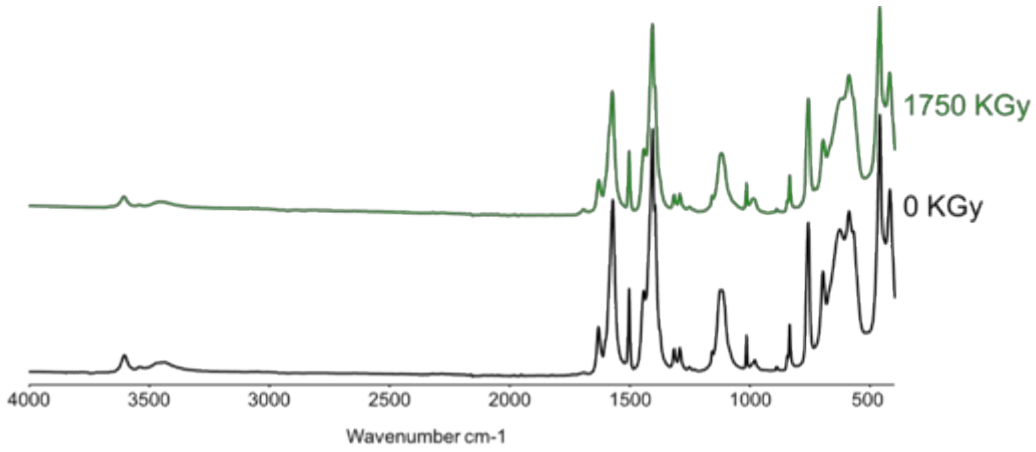

Figure S7a: Comparison of infrared spectra of non-irradiated and irradiated (1750 KGy) MIL-53(Al)

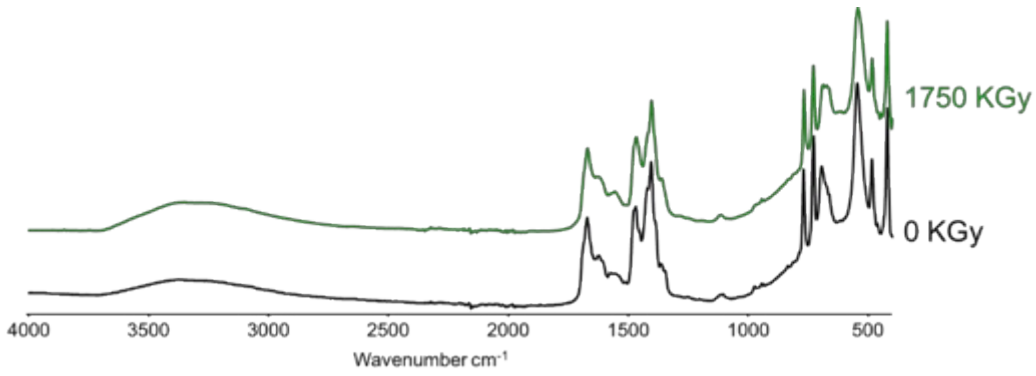

Figure S7b: Comparison of infrared spectra of non-irradiated and irradiated (1750 KGy) MIL-100(Al)

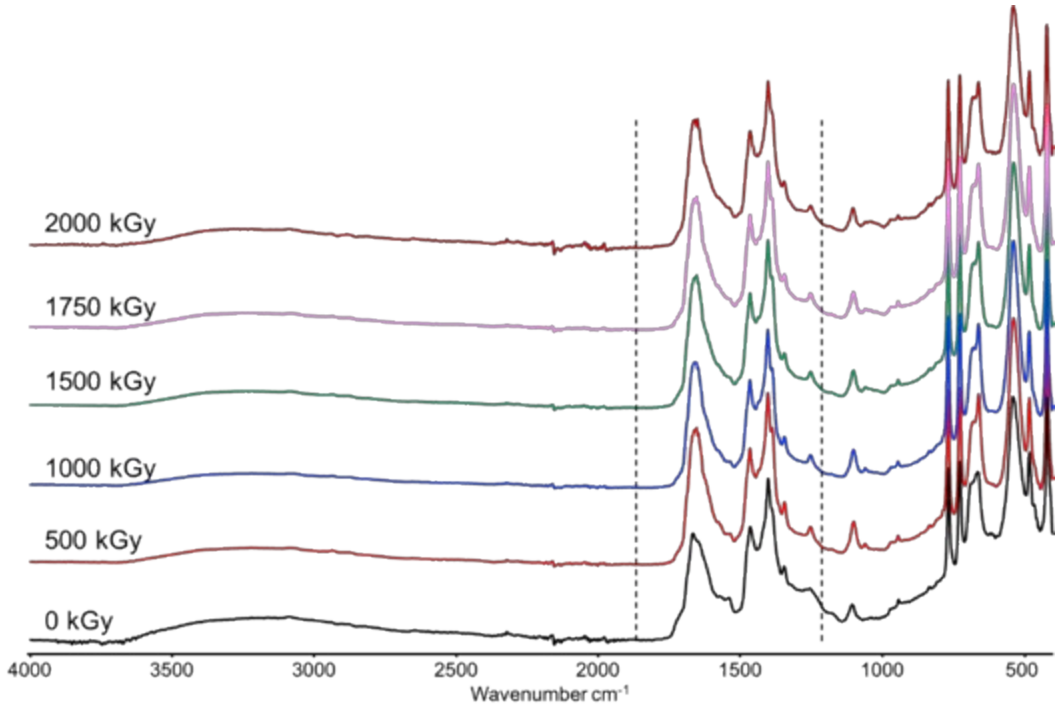

Figure S7c: Comparison of infrared spectra in the range 4000-400 cm^{-1}, of non-irradiated and irradiated (500 to 2000 kGy) MIL-100(Al)-as (as synthesized)

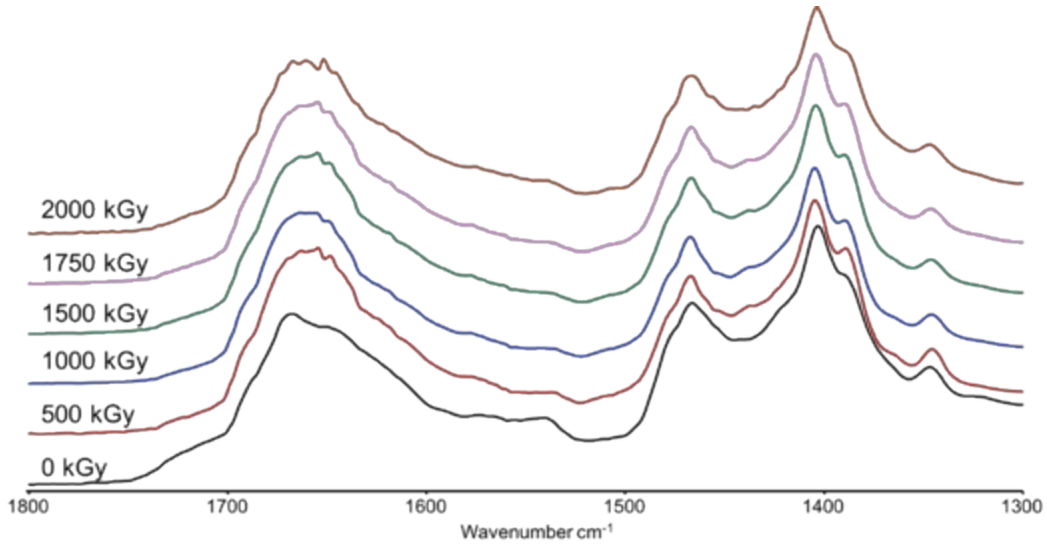

Figure S7d: Comparison of infrared spectra in the range 1300-800 cm^{-1}, of non-irradiated and irradiated (500 to 2000 kGy) MIL-100(Al)-as (as synthesized)

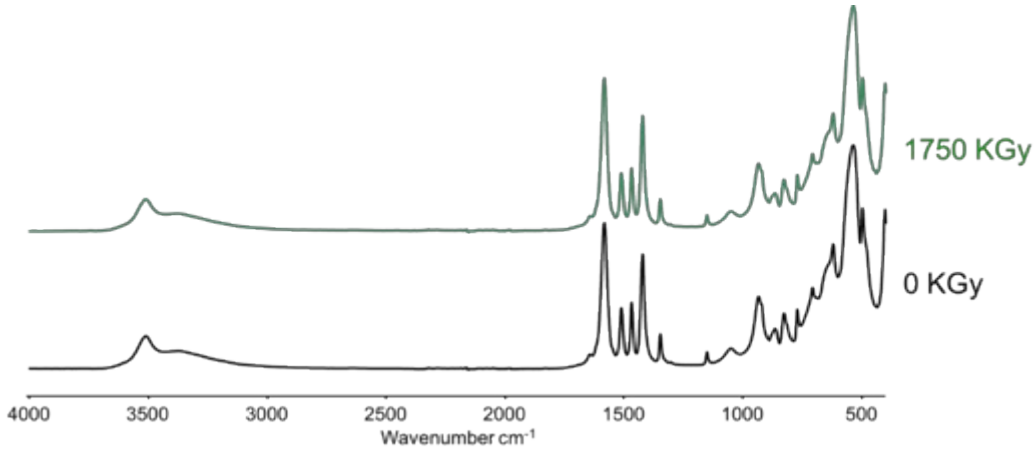

Figure S7e: Comparison of infrared spectra of non-irradiated and irradiated (1750 KGy) MIL-120(Al)

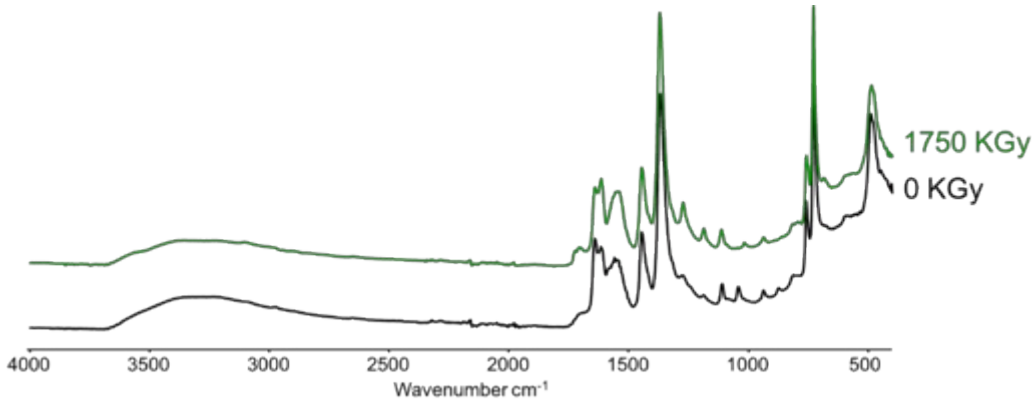

Figure S7f: Comparison of infrared spectra of non-irradiated and irradiated (1750 KGy) HKUST-1

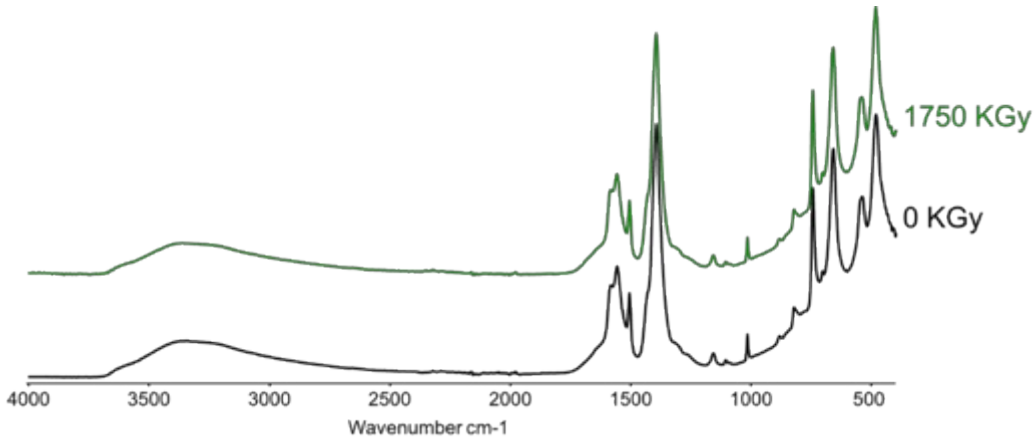

Figure S7g: Comparison of infrared spectra of non-irradiated and irradiated (1750 KGy) UiO-66(Zr)

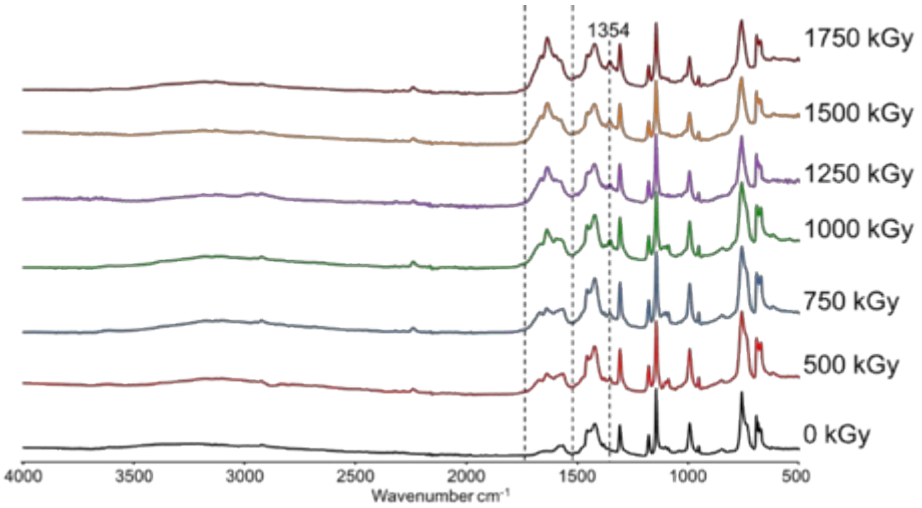

Figure S7h: Comparison of infrared spectra of non-irradiated and irradiated (500-1750 KGy) ZIF-8 (Zn)

Nuclear Magnetic Resonance

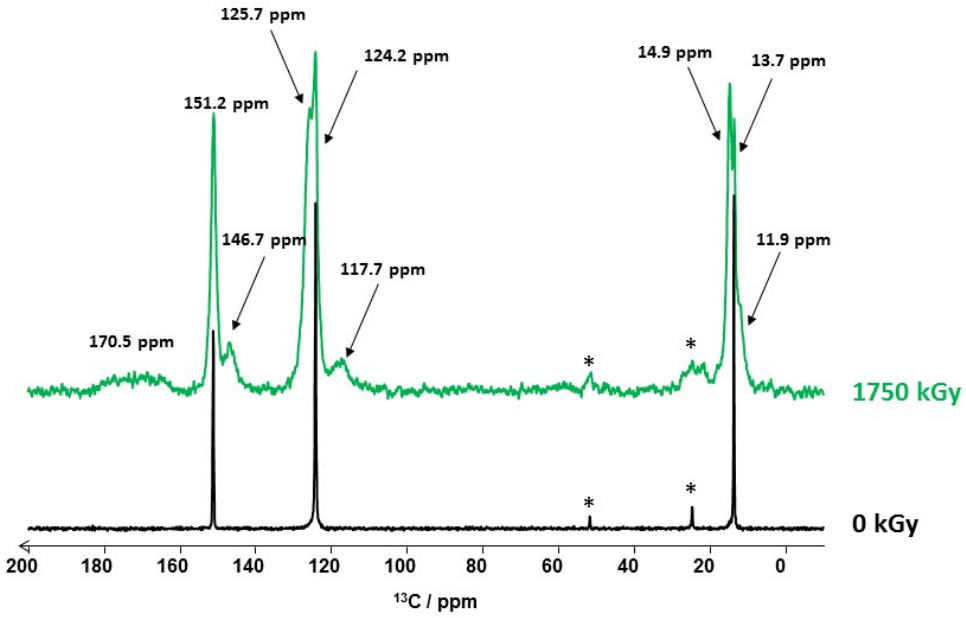

Figure S8a: Experimental $^{1}H \rightarrow ^{13}C$CPMAS NMR spectra of irradiated (1750 kGy) and non-irradiated (0 kGy) ZIF-8. An asterisk (*) indicates the spinning side bands

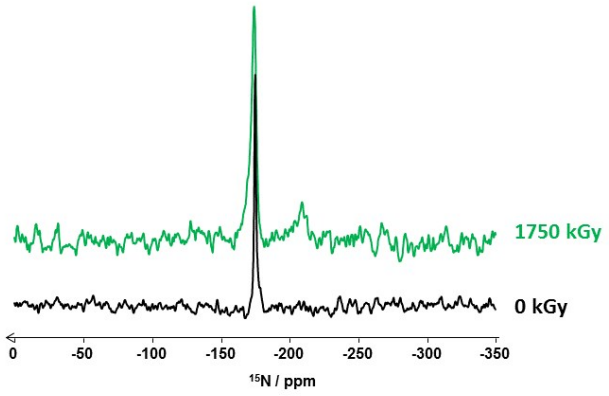

Figure S8b: Experimental $^{1}H \rightarrow ^{15}N$ CPMAS NMR spectra of irradiated (1750 kGy) and non-irradiated (0 kGy) ZIF-8

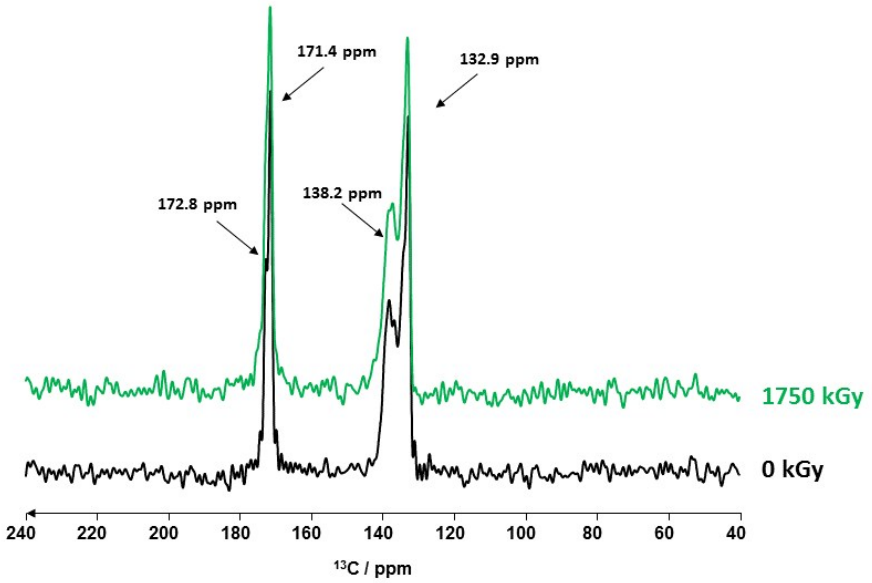

Figure S8c: Experimental $^{1}H \rightarrow ^{13}C$ CPMAS NMR spectra of irradiated (1750 kGy) and non-irradiated (0 kGy) MIL-100(Al)

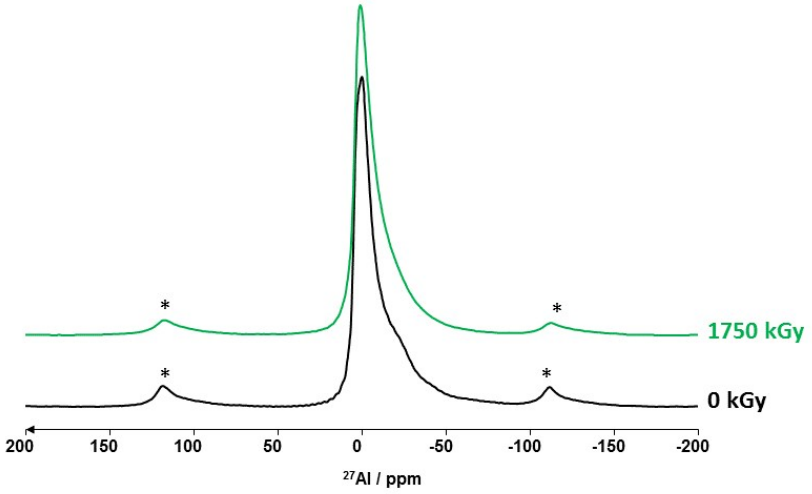

Figure S8d: Experimental ^{27}Al NMR spectra of irradiated (1750 kGy) and non-irradiated (0 kGy) MIL-100(Al)

References

1. Loiseau, T.; Serre, C.; Huguenard, C.; Fink, G.; Taulelle, F.; Henry, M.; Bataille, T.; Ferey, G., A rationale for the large breathing of the porous aluminum terephthalate (MIL-53) upon hydration. *Chemistry-a European Journal* **2004,** *10* (6), 1373-1382.

2. Volkringer, C.; Popov, D.; Loiseau, T.; Férey, G.; Burghammer, M.; Riekel, C.; Haouas, M.; Taulclle, F., Synthesis, Single-Crystal X-ray Microdiffraction, and NMR Characterizations of the Giant Pore Metal-Organic Framework Aluminum Trimesate MIL-100. *Chem. Mater.* **2009,** *21* (24), 5695-5697.

3. Volkringer, C.; Loiseau, T.; Haouas, M.; Taulelle, F.; Popov, D.; Burghammer, M.; Riekel, C.; Zlotea, C.; Cuevas, F.; Latroche, M.; Phanon, D.; Knofelv, C.; Llewellyn, P. L.; Férey, G., Occurrence of Uncommon Infinite Chains Consisting of Edge-Sharing Octahedra in a Porous Metal Organic Framework-Type Aluminum

Pyromellitate Al-4(OH)(8) C10O8H2 (MIL-120): Synthesis, Structure, and Gas Sorption Properties. *Chem. Mater.* **2009,** *21* (24), 5783-5791.
4. Chui, S. S. Y.; Lo, S. M. F.; Charmant, J. P. H.; Orpen, A. G.; Williams, I. D., A chemically functionalizable nanoporous material Cu-3(TMA)(2)(H2O)(3) (n). *Science* **1999,** *283* (5405), 1148-1150.
5. Park, K. S.; Ni, Z.; Cote, A. P.; Choi, J. Y.; Huang, R.; Uribe-Romo, F. J.; Chae, H. K.; O'Keeffe, M.; Yaghi, O. M., Exceptional chemical and thermal stability of zeolitic imidazolate frameworks. *Proc. Natl. Acad. Sci. U.S.A.* **2006,** *103* (27), 10186-10191.
6. Cavka, J. H.; Jakobsen, S.; Olsbye, U.; Guillou, N.; Lamberti, C.; Bordiga, S.; Lillerud, K. P., A new zirconium inorganic building brick forming metal organic frameworks with exceptional stability. *J. Am. Chem. Soc.* **2008,** *130* (42), 13850-13851.